Distinct regional meteorological influences on low cloud albedo susceptibility over global marine stratocumulus regions

Jianhao Zhang[1,2] and Graham Feingold[2]

[1]Cooperative Institute for Research in Environmental Sciences (CIRES), University of Colorado, Boulder, CO, USA
[2]Chemical Sciences Laboratory, National Oceanic and Atmospheric Administration (NOAA), Boulder, CO, USA

Key Points:

- Annual mean cloud brightening potential is the highest over subtropical coastal regions and the equatorial eastern Pacific.
- Features in regional relationships between key meteorological factors and albedo susceptibilities are absent in a global analysis.
- Monthly evolution of cloud radiative susceptibility and the co-varying large-scale meteorological conditions are regionally distinct.

Corresponding author: Jianhao Zhang, `jianhao.zhang@noaa.gov`

Abstract

Marine stratocumuli cool the Earth effectively due to their high reflectance of incoming solar radiation, and persistent occurrence. The susceptibility of cloud albedo to droplet number concentration perturbations depends strongly on large-scale meteorological conditions. Studies focused on the meteorological dependence of cloud adjustments often overlook the covariability among meteorological factors and their geographical and temporal variability. We use 8 years of satellite and reanalysis data sorted by day and geographical location to show that large-scale meteorological factors, including lower-tropospheric stability, free-tropospheric relative humidity, sea surface temperature, and boundary layer depth, have distinct covariabilities over each of the eastern subtropical ocean basins where marine stratocumulus prevail. This leads to markedly different monthly evolution in albedo susceptibility over each basin. Our results stress the importance of considering the geographical distinctiveness of temporal meteorological covariability when scaling up the local-to-global response of cloud albedo to aerosol perturbations.

Plain Language Summary

Bright, warm marine clouds help cool the Earth by reflecting a good fraction of sunlight. Their brightness is modulated by the amount of tiny particles in the air (aerosol) that can be induced by natural and/or human activities, e.g., volcanic eruptions and/or ship exhaust. Using 8 years of satellite observations, we show maps of potential cloud brightness changes associated with increases in the number of cloud droplets. The results suggest strong cloud brightening potential over subtropical coastal regions and weak darkening potential (reduction in cloud brightness) over some parts of the remote oceans. We find that the environmental conditions in which these cloud reside co-vary in time differently from one part of the world to another, leaving distinct regional fingerprints of cloud brightness changes. Such distinct fingerprints are not evident when data is aggregated globally. These findings imply that environmental conditions, especially the way they co-vary with each other, and their frequency of occurrence in space and time, is key to assessment of the overall brightness changes of marine low clouds.

1 Introduction

Marine warm (liquid) clouds cover about one third of the global ocean surface in annual mean (Chen et al., 2014). They prevail over low-latitude to mid-latitude oceans, more pronouncedly over the eastern subtropical oceans where the Earth's major semi-permanent marine stratocumulus decks form (Klein & Hartmann, 1993; Wood, 2012). These bright and blanket-like stratiform clouds reflect a good fraction of the incident solar radiation (ranging from 0.35 to 0.42 in annual mean; Bender et al., 2011) that would otherwise (in the absence of these clouds) be largely absorbed by the dark ocean ($\sim$94%), effectively cooling the Earth (e.g., Stephens et al., 2012). For warm clouds exhibiting constant macrophysical properties (e.g., liquid water path (LWP) and cloud cover), their brightness, or cloud albedo, quantified as the ratio of the reflected shortwave flux to the incoming solar radiation at the top of atmosphere, is particularly sensitive to the droplet concentration (N_d), such that higher N_d accompanied by smaller drops makes the cloud more reflective (cloud brightening; Twomey, 1974, 1977). However, cloud macrophysical properties do change with time as the system evolves, through precipitation, evaporation, and/or entrainment mixing processes (Wood, 2012). Microphysical changes in N_d and droplet sizes induced by aerosol perturbations can substantially modulate the rate and efficiency of these processes and thereby cause further adjustments in macrophysical properties and cloud albedo (e.g., Ackerman et al., 2004; Bretherton et al., 2007; Jiang et al., 2006).

In nature, the responses of cloud macrophysical properties to N_d perturbations are always complicated by the variability driven by local meteorology, and for decades, the

stated challenge and focus has been to untangle aerosol effects from covarying meteorological conditions (Stevens & Feingold, 2009). Simulations of marine boundary layer (MBL) clouds, in which meteorology can be easily controlled, indicate a bidirectional LWP adjustment to increasing N_d, such that for precipitating clouds, an increase in N_d induces smaller droplets that suppress condensate removal, eventually leading to an increase in LWP (brighter clouds; Albrecht, 1989), whereas for non-precipitating clouds, the reduced droplet sizes lead to weaker sedimentation fluxes at cloud tops,(Bretherton et al., 2007) and faster evaporation (Wang et al., 2003; Xue & Feingold, 2006), which both cause stronger entrainment mixing that reduce cloud LWP, resulting in less reflective clouds.

Observations of cloud adjustments following anthropogenic aerosol perturbations confirm the bidirectional LWP responses (e.g., Chen et al., 2012; Trofimov et al., 2020), while the aggregated response remains uncertain (Malavelle et al., 2017; Toll et al., 2019; Christensen et al., 2022). This means that cloud LWP responses to increased N_d can either enhance or offset the microphysical brightening depending on the meteorological conditions. Progress has been made over the years towards establishing fundamental knowledge of the environmental state/regime dependence of cloud adjustments to aerosol perturbations. For inversion-capped MBL clouds, the budget of cloud condensate is regulated mainly by entrainment drying at cloud tops and the fraction of precipitation that reaches the surface, which are strongly dependent on the humidity in the free-troposphere and the lower-tropospheric stability (Ackerman et al., 2004; Chen et al., 2014; Gryspeerdt et al., 2019). In part related to the atmospheric stability, clouds exhibit a much more negative LWP response to increased N_d in deep MBLs than those that reside in shallower MBLs (e.g., Possner et al., 2020; Toll et al., 2019). Furthermore, Dagan et al. (2015) show that the direction in which cloud condensate responds to an increase in aerosol depends on an optimal aerosol concentration which is determined by thermodynamic conditions (e.g., temperature and humidity). Wood (2007) shows that cloud-base height is the single most important determinant of whether cloud thickness changes will enhance or offset the Twomey brightening.

Clearly, the spatiotemporally integrated response of cloud albedo (A_c) to aerosol perturbations depends crucially on the frequency of occurrence of the environmental states that characterize cloud adjustments. However, we lack quantitative and even qualitative characterization of the way meteorological conditions influence aerosol effects in the real world. Mülmenstädt and Feingold (2018) state the need for a shift in attention from untangling aerosol effects from covarying meteorology towards embracing and understanding the covariabilities between them. The focus of this study is exactly on this point. In addition to characterizing the geographical distribution of warm cloud albedo susceptibility using satellite observations over global oceans from 60° S to 60° N, we illustrate the dependence of large-scale meteorological influences on albedo susceptibility in different stratocumulus basins (Section 4) and the role of temporal covariabilities in governing the observed susceptibility (Section 5); the latter are understudied and often ignored in "untangling" studies. We find distinct fingerprints (in terms of monthly evolution) of albedo susceptibility in different stratocumulus basins, consistent with the corresponding temporally covarying meteorological conditions. We show that a frequency-weighted aggregation of these regional fingerprints obscures these regional differences and therefore gives a biased view of albedo susceptibility.

2 Data and Methods

We obtain coincident marine low-cloud properties, including cloud optical depth (τ), cloud top effective radius (r_e), low-cloud fraction (f_c), cloud LWP, cloud top height (CTH), and top-of-atmosphere (TOA) shortwave (SW) fluxes from the MODerate resolution Imaging Spectroradiometer (MODIS) (Platnick et al., 2003) and the Clouds and the Earth's Radiant Energy Systems (CERES; Wielicki et al., 1996) sensors onboard the Terra and Aqua satellite (overpass ∼10:30 and ∼13:30 local time, respectively), which

are integrated into the CERES Single Scanner Footprint (SSF) product Edition 4 (level 2) with a footprint resolution of 20 km (Su et al., 2015). N_d is calculated following Zhang et al. (2022) for all CERES footprints with $f_c > 0.8$, in order to minimize retrieval biases (Grosvenor et al., 2018), while including some partially cloudy footprints. Footprint cloud properties are aggregated to 1° spatial resolution, to match susceptibilities calculated for individual 1° × 1° satellite snapshots. At this scale, the confounding effect of meteorology is negligible (Goren & Rosenfeld, 2012, 2014). Linear least-squares log-log regressions of footprint properties are used to calculate albedo susceptibility $S_0 = dln(A_c)/dln(N_d)$ and radiative susceptibility $F_0 = d(A_c)/dln(N_d) \times f_c \times SW_{dn}$; for both metrics, positive values indicate more reflected sunlight, thereby cooling, following Zhang et al. (2022). Note that in calculating S_0 we do not stratify by LWP. The logarithmic transformation alleviates the dependence of S_0 on the absolute value of N_d.

Meteorological conditions, including sea surface temperature (SST), lower tropospheric temperature, humidity, and wind profiles, are obtained from the European Centre for Medium-Range Weather Forecasts (ECMWF) fifth-generation atmospheric reanalysis (ERA5; Hersbach et al., 2020), and interpolated and aggregated to the Terra and Aqua overpass times at 1° spatial resolution. Lower-tropospheric-stability (LTS) is calculated as the difference in potential temperature between 700 hPa and 1000 hPa. Free-tropospheric relative humidity (RH_{ft}) is defined as the the mean relative humidity between inversion top and 700 hPa, following Eastman and Wood (2018).

The datasets span 60° S to 60° N, covering global oceans, from 2005 to 2012 (8 years). We screen for cloudy satellite scenes over open water when only single layer liquid cloud (SLLC) is present. Analyses using the Aqua observations are shown in the main text, and those using the Terra observations are shown in the supplementary material, in order to assess robustness of our findings (qualitatively), and to explore the role of the diurnal cycle (quantitatively). Regional annual maxima in SLLC fractional coverage and frequency of occurrence are used to identify 5 major marine stratus/stratocumulus regions (20° × 20°, Fig. S1, magenta boxes).

3 Global map of albedo susceptibility

The climatology of geographical distribution of marine low-cloud S_0 (Fig. 1a) is represented by an aggregation of susceptibilities derived from individual satellite snapshots over the 8-year period, taking into account the frequency of occurrence of different cloudy scenes and meteorological regimes. It is clear that over most parts of the global ocean (60° S to 60° N), low clouds have a brightening potential (positive S_0) in annual mean, more pronouncedly off the coast of continental land masses where N_d is climatologically higher (Fig. S2) and the MBL is shallower (Fig. S3), compared to those over remote oceans. Only over the remote subtropical southeast Pacific/Atlantic regions, do the data show weak darkening potential (negative S_0) in annual mean. The darkening potential means that the brightening of the clouds via the Twomey effect – i.e., more particles lead to more droplets and brighter clouds – is more than compensated by liquid water losses.

One can then translate the S_0 map into an annual flux perturbation potential map (Fig. 1b), which highlights the high annual cooling potential over subtropical stratocumulus regions even more, by taking into account the cloud fraction and frequency and amount of incoming solar radiation at a given geographical location. In the remote parts of the subtropical stratocumulus decks, warmer SSTs deepen the MBL and encourage entrainment of free-tropospheric air at cloud tops (Fig. S3 and Bretherton, 1992; Wyant et al., 1997), favoring entrainment-feedback-driven LWP decreases with increasing N_d (Bretherton et al., 2007; Wang et al., 2003). The prevalence of this MBL condition leads to a frequently occurring cloud darkening regime that offsets the Twomey brightening,

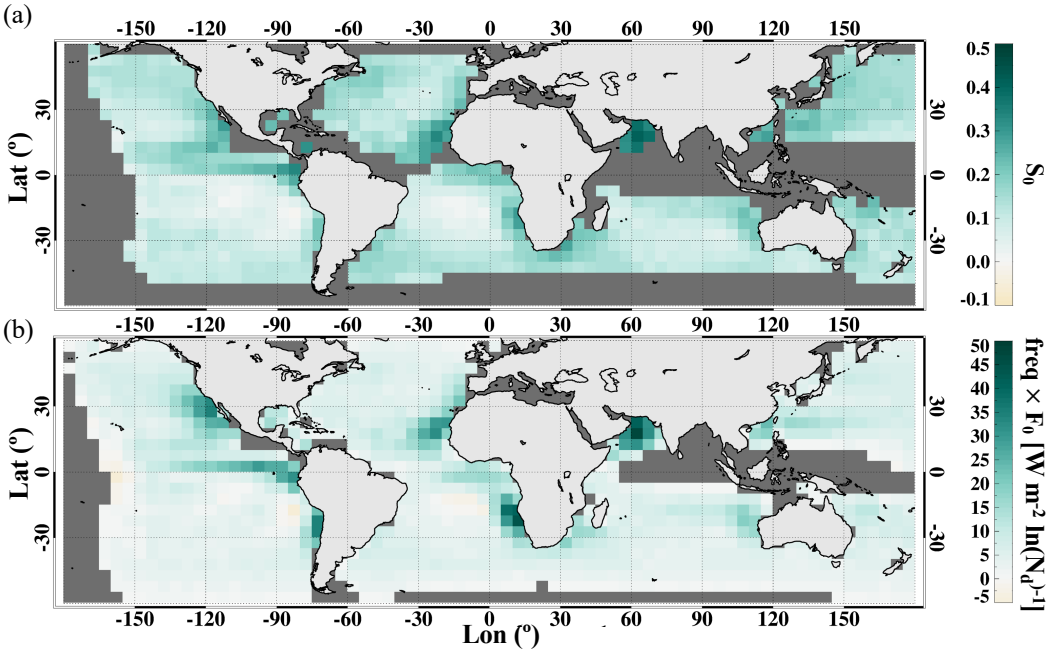

Figure 1. Geographical distribution of marine low-cloud (a) albedo susceptibility (S_0) and (b) the product of radiative susceptibility (F_0) and annual frequency of occurrence of single layer liquid cloud (SLLC). Spatial-temporal averages of 5° × 5° areas are shown. Only areas with SLLC frequency of occurrence greater than 0.1 are shown in (a).

consistent with the net warming potential observed over the southeast Pacific/Atlantic (Fig. 1b).

Contributions from the three susceptibility regimes, namely non-precipitating brightening, darkening, and precipitating brightening, to the total F_0 are observed to have distinct geographical preferences (Fig. 2). The regime separation is performed for each 5° × 5° area to ensure robustness, based on the sign of S_0 and a r_e of 12 μm (above which clouds are more likely to drizzle) that manifest in the LWP-N_d variable space, similarly to Zhang et al. (2022). Each regime represents a cluster of cloud states that is dominated by brightening or darkening, and precipitating or non-precipitating potentials. Contributions from the non-precipitating brightening cloud states tend to dominate the shallow, often polluted, stratus/stratocumulus off the coast of continents (Fig. 2a). The precipitating brightening cloud states, attributed to rain suppression (Albrecht, 1989), contribute substantially over most parts of the remote, clean oceans and the equatorial eastern Pacific (Fig. 2c). Inbetween the geographical preferences of the above two regimes lies the region where non-precipitating darkening cloud states become the leading contributor to the overall F_0, especially over the southeast Pacific and Atlantic (Fig. 2b), where net warming potentials are observed (Fig. 1).

4 Distinct fingerprints of S_0 in meteorological space at regional scale

Local adjustments of low clouds to aerosol perturbations are strongly dependent on the depth of the stratocumulus-topped MBL (approximated by CTH; e.g., Possner et al., 2020; Toll et al., 2019) and RH_{ft} (e.g., Chen et al., 2014; Gryspeerdt et al., 2019). Figure 3 shows S_0 under different MBL and free-troposphere (FT) states, as a function of CTH and RH_{ft}. Globally (60° S - 60° N), positive S_0 is found everywhere across the

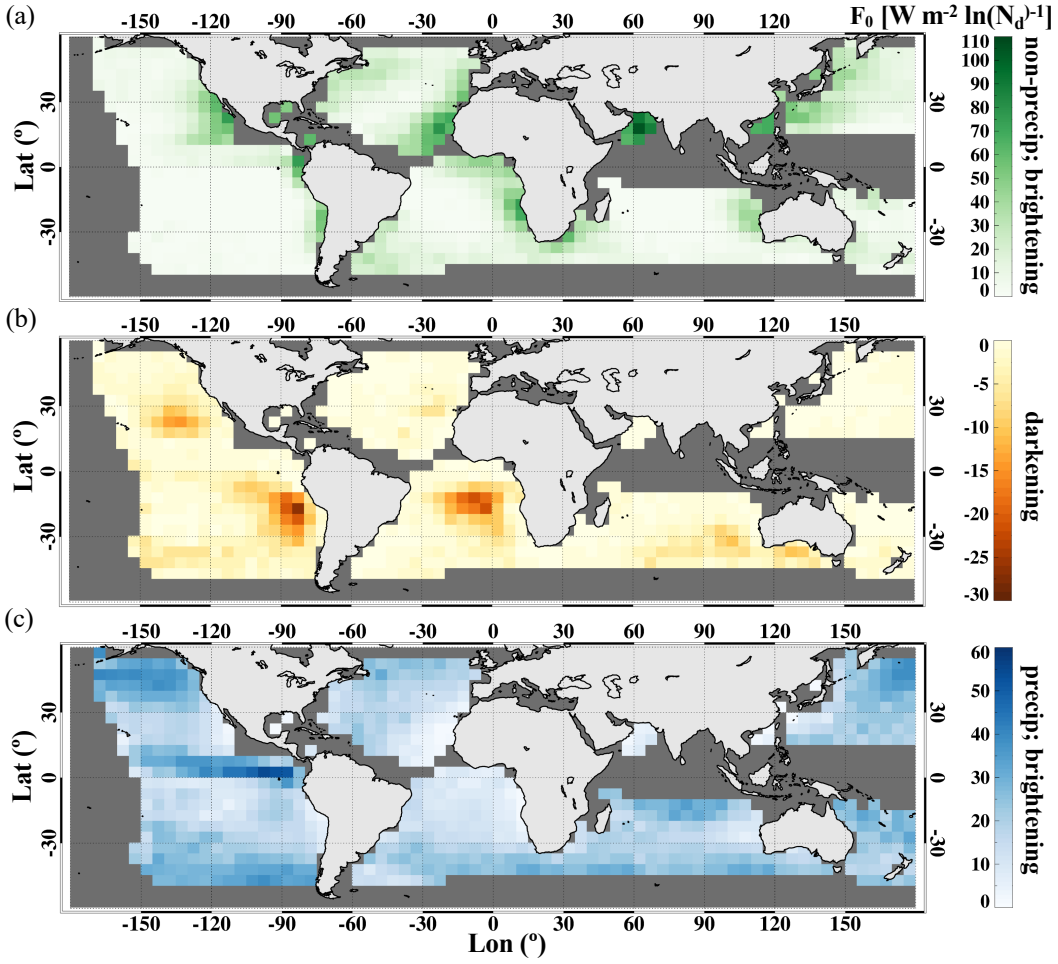

Figure 2. Geographical distribution of marine low-cloud radiative susceptibility (F_0) separated into 3 regimes: (a) non-precipitating brightening, (b) darkening, and (c) precipitating brightening. The 3 regimes are separated based on the sign of S_0 and a r_e of 12 μm in the LWP-N_d variable space, for each 5° × 5° area, similarly to Zhang et al. (2022). Only areas with SLLC frequency of occurrence greater than 0.1 are shown.

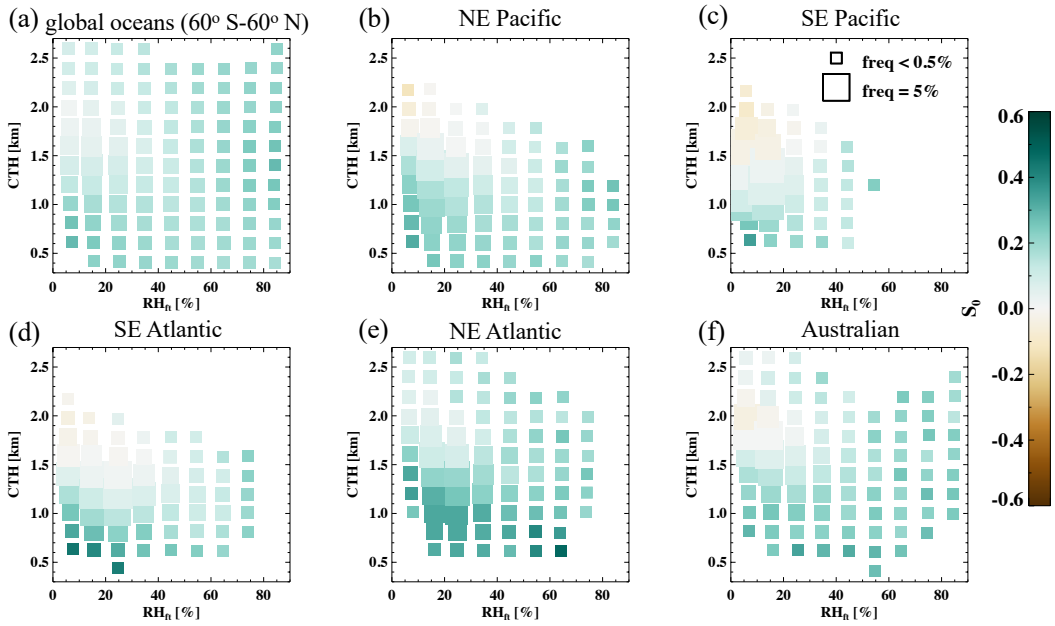

Figure 3. Mean S_0 under different meteorological conditions, namely free-tropospheric relative humidity (RH_{ft}; x-axis) and cloud top height (CTH; y-axis; a proxy for the marine boundary layer depth), for (a) global oceans (60° S - 60° N), (b) NE Pacific, (c) SE Pacific, (d) SE Atlantic, (e) NE Atlantic, and (f) Australian stratocumulus regions. Bin sizes for CTH and RH_{ft} are 0.2 km and 10%, respectively. The size of the square indicates the frequency of occurrence of a meteorological state. Bins with less than 0.1% frequency of occurrence (or less than 100 samples) are not shown.

two meteorological state-spaces, with less susceptible conditions occurring under drier FT and intermediate MBL depth (∼1.5 km; Fig. 3a). This is consistent with the entrainment feedback argument that reduced droplet sizes and the subsequent reduced cloud-top sedimentation flux enhance evaporation and thereby cloud-top entrainment mixing (Bretherton et al., 2007; Xue & Feingold, 2006), which is further facilitated by the deeper MBL and the drier air above cloud tops. Cloud brightening potentials associated with rain-suppression overwhelm these entrainment-feedback-consistent signals, as the clouds become even deeper (>2 km) and are more likely to precipitate (Fig. 3a).

When the stratocumulus regime is singled out (Fig. 3b-f), the S_0 distribution in the two meteorological states is in qualitative agreement with the global analysis, however, cloud darkening (negative S_0) appears under the deep-MBL, dry-FT atmospheric states, more pronouncedly over the southeast Pacific stratocumulus deck (Fig. 3c), while weak brightening potential is observed under those conditions over the NE Atlantic (Fig. 3e). This is likely because clouds over the NE Atlantic precipitate more often than those over the SE Pacific, under these MBL and FT conditions (discussed further in Section 5).

Distinct "fingerprints" of S_0 in the CTH-RH_{ft} variable space are evident, when individual basins are being compared. This manifests in two ways; first, the frequency of occurrence (indicated by the square sizes) of the FT and MBL conditions varies from basin to basin. For example, deep MBL (>2 km) or humid FT conditions rarely occur under the large-scale subsidence-dominated regions (Fig. 3b-d), compared to the NE Atlantic or the Australian basins (Fig. 3e-f). Second, different S_0, at least in magnitude, and in some cases even in sign, are observed across basins. This suggests cloud states (defined in LWP, N_d space) are not necessarily the same for the same MBL and FT states, implying that other meteorological factors co-evolve with MBL and FT states differently from region to region, leaving distinct imprints on S_0. These distinct regional fingerprints of S_0-meteorology relationships are lost in the global analysis (Fig. 3a) due to the merging of different cloud/meteorology regimes besides MBL depth and RH_{ft}.

5 Seasonal covariability between albedo susceptibility and large-scale meteorology

Four key large-scale meteorological factors evolve and co-vary distinctly across basins (Fig. 4, right column), leading to markedly different monthly evolution in F_0 (Fig. 4, left column). Even among regions strongly influenced by large-scale subsidence (Fig. 4a-c), large-scale meteorological conditions vary in magnitude and do not covary the same way temporally (e.g., RH_{ft} tracks SST except over the SE Atlantic, LTS anti-correlates with SST except over the NE Pacific). As a result of the complex and distinct regional covariability in meteorological conditions, the temporal rise and fall of a single meteorological factor leads to markedly different responses in F_0 across basins. For instance, when SST peaks over the NE Pacific, F_0 is at its annual minimum, owing to the coincident relatively strong LTS, keeping the high-LWP (color of the circle) clouds from deepening-precipitating while being susceptible to entrainment drying (Fig. 4a, Jul–Aug). In contrast, over the Australian stratus region, the annual maximum in F_0 coincides with the warmest SST, owing to enhanced Twomey brightening potential associated with more frequent non-precipitating conditions, compared to the other months over this region (Fig. 4e, Feb). Taking CTH as another example, high CTHs (deep MBLs) lead to strong precipitation-suppression brightening over the NE Atlantic, whereas deep MBLs over the SE Pacific show very weak brightening potentials, due to high stability and dry FT conditions, in striking contrast to the NE Atlantic (Fig. 4b and d).

The covariability among large-scale meteorological factors over the SE Atlantic follows that over the SE Pacific, although the ocean surface is warmer, LTS is weaker, and the FT is moister in general over the SE Atlantic (Fig. 4c). This leads to qualitatively

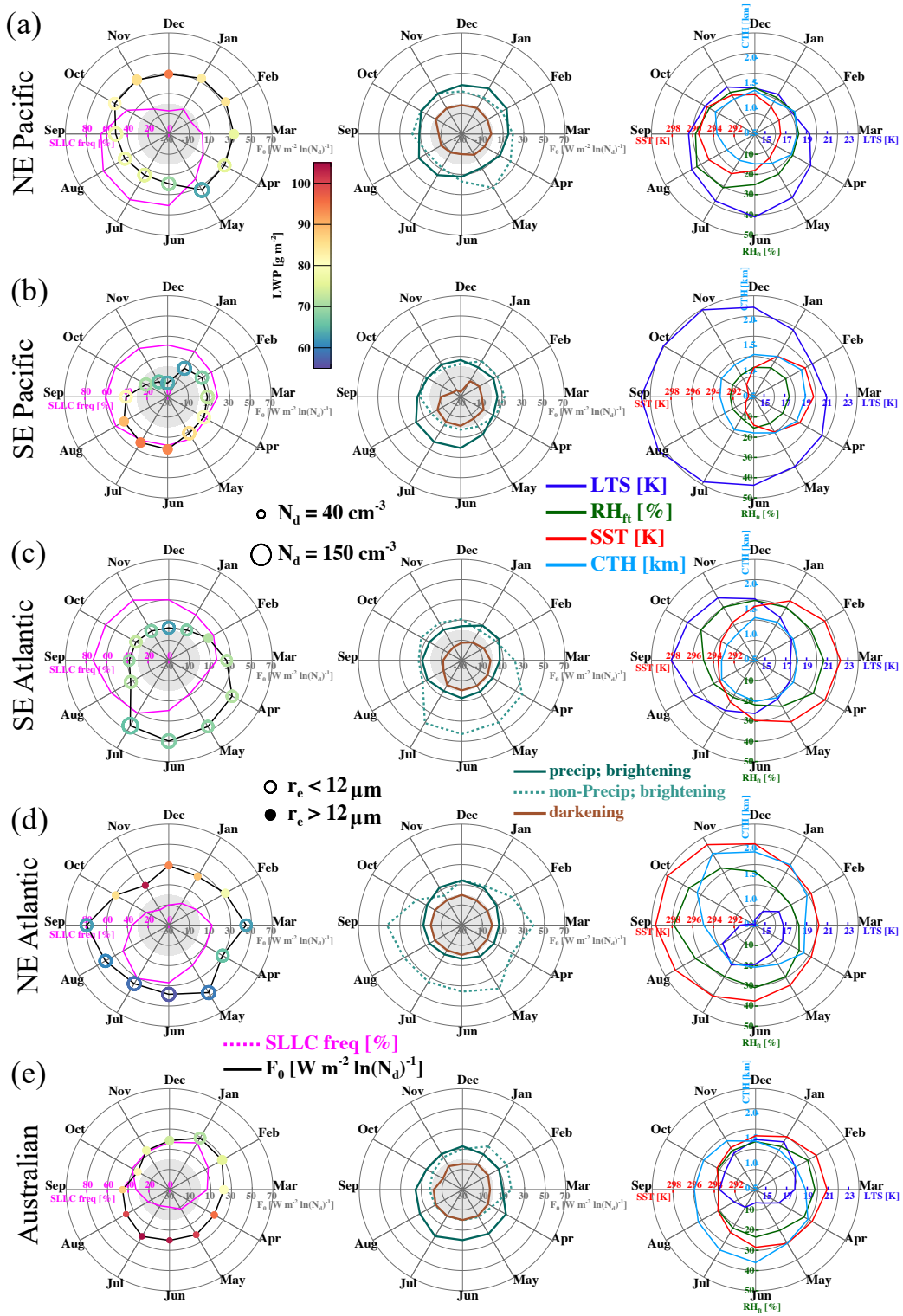

Figure 4. Left column: Monthly mean radiative susceptibility (F_0; black; positive values indicate cooling) and frequency of occurrence of SLLC (magenta). Color of the circle indicates monthly mean LWP. Size of the circle indicates monthly mean N_d. Open (closed) circles indicate likely precipitating (non-precipitating) condition, based on $r_e = 12$ μm. **Middle column:** Monthly mean F_0 broken into 3 regimes: non-precipitating brightening (dotted green), darkening (brown), and precipitating brightening (solid green). **Right column:** Monthly mean meteorological conditions: LTS (blue), RH_{ft} (dark green), SST (red), and CTH (cyan). Rows (a–e) represent results for the NE Pacific, SE Pacific, SE Atlantic, NE Atlantic, and the Australian stratocumulus regions, respectively.

similar F_0 evolutions between the two basins; that is high F_0 during austral winter and low F_0 during austral summer. An exception occurs during late fall to winter (June-July), when precipitating clouds over the SE Pacific exhibit relatively weak positive F_0 whereas non-precipitating high N_d clouds occur and exhibit strong F_0 over the SE Atlantic. This difference can be attributed to an aerosol source that is unique to the SE Atlantic basin, in the form of a large amount of biomass burning aerosol that is advected by the co-occurring African Easterly Jet in the FT during the southern African burning season (June-October; Adebiyi & Zuidema, 2016). The elevated aerosol is likely to be entrained into the MBL during June-July when the FT jet is not yet at its full strength (Zhang & Zuidema, 2021).

Among five subtropical stratocumulus/stratus regions, the SE Pacific hosts the least susceptible conditions overall and is the only basin with monthly mean cloud darkening potential (Fig. 4b). This is attributed to the extremely dry free-tropospheric conditions, under which entrainment feedbacks acting to reduce cloud LWP, and associated with reduced droplet sizes (due to increasing aerosol) are enhanced. Low clouds over the NE Atlantic indicate the highest cloud brightening potential among the five regions, especially during March-September when the MBL is shallow and FT is relatively moist, giving rise to thin, non-precipitating clouds with low LWP, relatively high N_d, and the lowest entrainment-driven cloud darkening potential (Fig. 4d). During October-February over the NE Atlantic, when CTH is high (deep MBL), clouds precipitate often, leading to a high potential for precipitation-suppression related cloud brightening. Given the deep MBLs, precipitating conditions occur fairly frequently over the Australian stratus region almost throughout the year, except for the January-March period when increasing LTS leads to lower LWP and shallower MBL (Fig. 4e). This leads to an almost all-year-round precipitation-suppression driven cloud brightening potential, enhanced during the January-March period with a contribution from the non-precipitating brightening.

Albedo susceptibility, cloud frequency and areal coverage, and aerosol conditions (indicated by N_d) collectively determine the SW flux budget at TOA in response to an aerosol perturbation. The temporal covariability among these variables (Fig. 4, left column) can lead to a muted SW flux perturbation even when highly susceptible clouds occur, due to a coinciding low frequency of cloud occurrence and/or high aerosol conditions (e.g., the NE Pacific and the SE Atlantic). This stresses the necessity of taking such temporal covariability into account when assessing the climatological radiative effect of aerosol-cloud interactions. Furthermore, not only do various spatial-temporal averages applied in satellite-based approaches lead to biased susceptibilities (Feingold et al., 2022), temporal covariabilities among multiplicands (F_0, cloud frequency, and aerosol condition) also bias their product (TOA SW flux perturbation) if temporal averages are applied to multiplicands before multiplication (Fig. S4). Biases associated with individual stratocumulus regions vary in sign and magnitude, indicating that these quantities do not necessarily co-vary the same way temporally across basins (e.g., the NE versus SE Pacific).

6 Discussion and implications

To illustrate our findings in a conceptual framework one may ideally construct a manifold that depicts S_0 in a 4-dimensional (SST, CTH, RH_{ft}, and LTS) space by populating the 4-D space with a large body of realizations, i.e., climatological observations. However, often ignored is that each realization used to construct the 4-D manifold is associated with a specific combination of longitude, latitude, and time. In other words, given a certain geographical region and time, realizations will only populate parts of the 4-D space, leading to local constructions (distinct fingerprints) that looks different from a global construction.

Our work is highly relevant to assessment of the radiative effect of aerosol-cloud interactions for climate applications. In addition, our findings have direct implications

for Marine Cloud Brightening (MCB), which has been proposed as a way to mitigate the worst effects of the ongoing global warming crisis by creating more reflective (in the SW) MBL clouds, ideally with expanded areal coverage and prolonged lifetime, through deliberate aerosol injections (Latham et al., 2012). The bright, linear cloud features seen in satellite images, referred to as ship tracks (Coakley et al., 1987), are examples of ideal outcomes of an MCB experiment, and the conditionality of such an outcome on meteorological conditions is one of the key issues underpinning the viability of MCB. This study underscores two key points for the MCB community: 1) understanding or evaluating the impact of meteorology on cloud albedo susceptibility needs to be done at local/regional scales, where meteorological covariability is accounted for; 2) When scaling up the flux perturbation, it is crucial to consider the natural covariability between meteorology and aerosol, to which cloud responses to aerosol perturbation are sensitive.

Last but not least, S_0 and the regime-specific F_0 derived from the morning observations (Terra; Fig. S5-S6) have the same geographical distributions as those observed in the afternoon (Aqua; Fig. 1-2), except that Terra observations indicate a slightly higher global mean S_0 of 0.14, compared to 0.13 for Aqua observations. While the qualitative distributions of S_0 in the CTH-RH_{ft} state space remain the same, regardless of the observing time (morning versus afternoon), the morning observations (Terra; Fig. S7) do indicate a general shift towards $S_0 > 0$, which replaces the cloud darkening regime related to the deep-MBL dry-FT conditions (Fig. 3) with a weak brightening regime. This stresses the importance of cloud diurnal evolution for S_0 in that the same meteorological conditions may lead to opposing susceptibility regimes (i.e., brightening versus darkening) depending on the time of the day. Except for generally higher cloud LWP and higher F_0, the characterized covariability among cloud LWP, N_d, SLLC frequency of occurrence, F_0, and large-scale meteorological conditions using the Terra observations agrees well with those using the Aqua observations (Fig. S8 and Fig. 4).

7 Concluding Remarks

Marine warm cloud albedo susceptibility is derived from satellite-retrieved cloud microphysical properties and radiative fluxes, and sorted by day and geographical location. Geographical distributions of albedo susceptibility and the contributions from three susceptibility regimes (non-precipitating brightening, darkening, precipitating brightening) are shown over global oceans (60° S to 60° N). Monthly evolutions in cloud radiative susceptibility, meteorological conditions (from ERA5 reanalysis), warm cloud frequency of occurrence, LWP and N_d are shown for five primary eastern subtropical stratus/stratocumulus regions (20° × 20°), to illustrate the covariabilities among them. The key findings are as follows:

1. An overall annual mean cloud brightening potential is observed for global marine warm clouds – most pronounced over subtropical coastal regions where shallow marine stratocumulus prevail along with high annual-mean N_d, and over the equatorial eastern Pacific where clouds rain more often (Fig. 1).
2. Cloud darkening associated with entrainment-driven negative LWP adjustments offsets the cloud brightening potential over remote parts of the stratocumulus regions where deeper MBLs favor cloud top entrainment, especially over the SE Pacific/Atlantic where darkening overcomes brightening in annual mean (Fig. 1 and Fig. 2).
3. The distinct regional fingerprints of S_0 in CTH and RH_{ft} variable space are absent in the global analysis because the latter merges different cloud/meteorology regimes (Fig. 3).
4. Meteorological conditions have distinct regional covariabilities, leading to markedly different monthly evolutions in F_0 (Fig. 4).

5. The SE Pacific, a region with the driest free-tropospheric conditions, hosts the least susceptible clouds exhibiting cloud darkening potential over several months during austral winter. Frequently occurring non-precipitating low-LWP, high-N_d clouds, found in shallow MBLs (March-September) over the NE Atlantic, represent the highest potential radiative responses to N_d perturbations among the five stratocumulus regions (Fig. 4).
6. While the qualitative agreement between Terra and Aqua underscores the robustness of our findings, their quantitative disagreement points to the important role of cloud diurnal evolution in determining albedo susceptibility (Figs S5-S8).

When the influence of meteorological conditions on low cloud S_0 are studied, it may seem tempting to try to disentangle effects of individual meteorological factors on S_0 by controlling for the others. Our results, however, indicate that this may not be the best approach since it is the natural covariability among meteorological conditions that dictates the regionally distinct temporal evolution in S_0. These results convey the importance of spatiotemporal variability in S_0 as a basis for both understanding the limitation in scale-up of the meteorological influences on the radiative effect of aerosol-cloud interactions from regional to global, as well as for making decisions regarding when, where, and if marine cloud brightening efforts should be attempted.

Acknowledgments

This research has been supported in part by the U.S. Department of Energy, Office of Science, Atmospheric System Research Program Interagency Award 89243020SSC000055, the U.S. Department of Commerce, Earth's Radiation Budget grant, NOAA CPO Climate & CI #03-01-07-001, and the NOAA Cooperative Agreement with CIRES, NA17OAR4320101. We thank the two anonymous reviewers for their constructive comments and suggestions that helped us improve the original paper.

Data Availability Statement

The CERES SSF data were obtained from the Atmospheric Science Data Center at the NASA Langley Research Center (`https://asdc.larc.nasa.gov/project/CERES/CER_SSF_Aqua-FM4-MODIS_Edition4A`; NASA/LARC/SD/ASDC (2014a); `https://asdc.larc.nasa.gov/project/CERES/CER_SSF_Terra-FM2-MODIS_Edition4A`; NASA/LARC/SD/ASDC (2014b)). The fifth-generation ECMWF (ERA5) atmospheric reanalyses of the global climate data are available through the Copernicus Climate Change Service (C3S, `https://doi.org/10.24381/cds.bd0915c6`; Hersbach et al. (2020)). The 1° albedo susceptibility data derived and shown in this study can be found at `https://csl.noaa.gov/groups/csl9/datasets/data/cloud_phys/2022-Zhang-Feingold/`.

References

Ackerman, A. S., Kirkpatrick, M. P., Stevens, D. E., & Toon, O. B. (2004). The impact of humidity above stratiform clouds on indirect aerosol climate forcing. *Nature*, *432*, 1014–1017.

Adebiyi, A. A., & Zuidema, P. (2016). The role of the southern African easterly jet in modifying the southeast Atlantic aerosol and cloud environments. *Quarterly Journal of the Royal Meteorological Society*, *142*(697), 1574–1589. doi: 10.1002/qj.2765

Albrecht, B. A. (1989). Aerosols, cloud microphysics, and fractional cloudiness. *Science*, *245*(4923), 1227–1230. doi: 10.1126/science.245.4923.1227

Bender, F. A.-M., Charlson, R. J., Ekman, A. M. L., & Leahy, L. V. (2011). Quantification of monthly mean regional scale albedo of marine stratiform clouds in satellite observations and gcms. *Journal of Applied Meteorology and Climatol-*

ogy, *50*(10), 2139–2148. doi: 10.1175/JAMC-D-11-049.1

Bretherton, C. S. (1992). A conceptual model of the stratocumulus-trade-cumulus transition in the subtropical oceans. *Proceeding of the11th International Conference on Clouds and Precipitation*, *vol. 1*, pp. 374–377.

Bretherton, C. S., Blossey, P. N., & Uchida, J. (2007). Cloud droplet sedimentation, entrainment efficiency, and subtropical stratocumulus albedo. *Geophysical Research Letters*, *34*, L03813. doi: https://doi.org/10.1029/2006GL027648

Chen, Y.-C., Christensen, M., Stephens, G. L., & Seinfeld, J. H. (2014). Satellite-based estimate of global aerosol–cloud radiative forcing by marine warm clouds. *Nature Geosciences*, *7*, 643–646. doi: 10.1038/ngeo2214

Chen, Y.-C., Christensen, M. W., Xue, L., Sorooshian, A., Stephens, G. L., Rasmussen, R. M., & Seinfeld, J. H. (2012). Occurrence of lower cloud albedo in ship tracks. *Atmos. Chem. Phys.*, *12*(17), 8223–8235. Retrieved from `https://acp.copernicus.org/articles/12/8223/2012/` doi: 10.5194/acp-12-8223-2012

Christensen, M. W., Gettelman, A., Cermak, J., Dagan, G., Diamond, M., Douglas, A., ... Yuan, T. (2022). Opportunistic experiments to constrain aerosol effective radiative forcing. *Atmospheric Chemistry and Physics*, *22*(1), 641–674. doi: 10.5194/acp-22-641-2022

Coakley, J. A., Bernstein, R. L., & Durkee, P. A. (1987). Effect of ship-stack effluents on cloud reflectivity. *Science*, *237*(4818), 1020–1022. doi: 10.1126/science.237.4818.1020

Dagan, G., Koren, I., & Altaratz, O. (2015). Competition between core and periphery-based processes in warm convective clouds – from invigoration to suppression. *Atmospheric Chemistry and Physics*, *15*(5), 2749–2760. doi: 10.5194/acp-15-2749-2015

Eastman, R., & Wood, R. (2018). The competing effects of stability and humidity on subtropical stratocumulus entrainment and cloud evolution from a lagrangian perspective. *Journal of the Atmospheric Sciences*, *75*(8), 2563–2578. doi: 10.1175/JAS-D-18-0030.1

Feingold, G., Goren, T., & Yamaguchi, T. (2022). Quantifying albedo susceptibility biases in shallow clouds. *Atmospheric Chemistry and Physics*, *22*(5), 3303–3319. doi: 10.5194/acp-22-3303-2022

Goren, T., & Rosenfeld, D. (2012). Satellite observations of ship emission induced transitions from broken to closed cell marine stratocumulus over large areas. *Journal of Geophysical Research: Atmospheres*, *117*(D17). doi: https://doi.org/10.1029/2012JD017981

Goren, T., & Rosenfeld, D. (2014). Decomposing aerosol cloud radiative effects into cloud cover, liquid water path and twomey components in marine stratocumulus. *Atmos. Res.*, *138*, 378–393. doi: https://doi.org/10.1016/j.atmosres.2013.12.008

Grosvenor, D. P., Sourdeval, O., Zuidema, P., Ackerman, A., Alexandrov, M. D., Bennartz, R., ... Quaas, J. (2018). Remote sensing of droplet number concentration in warm clouds: A review of the current state of knowledge and perspectives. *Reviews of Geophysics*, *56*(2), 409–453. doi: 10.1029/2017RG000593

Gryspeerdt, E., Goren, T., Sourdeval, O., Quaas, J., Mülmenstädt, J., Dipu, S., ... Christensen, M. (2019). Constraining the aerosol influence on cloud liquid water path. *Atmospheric Chemistry and Physics*, *19*(8), 5331–5347. doi: 10.5194/acp-19-5331-2019

Hersbach, H., Bell, B., Berrisford, P., Hirahara, S., Horányi, A., Muñoz-Sabater, J., ... Thépaut, J.-N. (2020). The ERA5 global reanalysis. *Quarterly Journal of the Royal Meteorological Society*, *146*(730), 1999–2049. doi: 10.1002/qj.3803

Jiang, H., Xue, H., Teller, A., Feingold, G., & Levin, Z. (2006). Aerosol effects on the lifetime of shallow cumulus. *Geophysical Research Letters*, *33*, L14806. doi:

https://doi.org/10.1029/2006GL026024

Klein, S. A., & Hartmann, D. L. (1993). The seasonal cycle of low stratiform clouds. *Journal of Climate*, *6*(8), 1587–1606. doi: 10.1175/1520-0442(1993)006⟨1587:TSCOLS⟩2.0.CO;2

Latham, J., Bower, K., Choularton, T., Coe, H., Connolly, P., Cooper, G., ... Wood, R. (2012). Marine cloud brightening. *Philosophical Transactions of the Royal Society A: Mathematical, Physical and Engineering Sciences*, *370*(1974), 4217–4262. doi: 10.1098/rsta.2012.0086

Malavelle, F. F., Haywood, J. M., Jones, A., Gettelman, A., Clarisse, L., Bauduin, S., ... Thordarson, T. (2017). Strong constraints on aerosol-cloud interactions from volcanic eruptions. *Nature*, *546*, 485–491. doi: 10.1038/nature22974

Mülmenstädt, J., & Feingold, G. (2018). The radiative forcing of aerosol–cloud interactions in liquid clouds: Wrestling and embracing uncertainty. *Current Climate Change Reports*, *4*, 23–40. doi: 10.1007/s40641-018-0089-y

NASA/LARC/SD/ASDC. (2014a, 10 2). *Ceres single scanner footprint (ssf) toa/surface fluxes, clouds and aerosols aqua-fm4 edition4a.* NASA Langley Atmospheric Science Data Center DAAC. Retrieved from `https://doi.org/10.5067/AQUA/CERES/SSF-FM4_L2.004A`

NASA/LARC/SD/ASDC. (2014b, 10 2). *Ceres single scanner footprint (ssf) toa/surface fluxes, clouds and aerosols terra-fm2 edition4a.* NASA Langley Atmospheric Science Data Center DAAC. Retrieved from `https://doi.org/10.5067/TERRA/CERES/SSF-FM2_L2.004A`

Platnick, S., King, M. D., Ackerman, S. A., Menzel, W. P., Baum, B. A., Riedi, J. C., & Frey, R. A. (2003). The MODIS cloud products: algorithms and examples from Terra. *IEEE Transactions on Geoscience and Remote Sensing*, *41*(2), 459–473. doi: 10.1109/TGRS.2002.808301

Possner, A., Eastman, R., Bender, F., & Glassmeier, F. (2020). Deconvolution of boundary layer depth and aerosol constraints on cloud water path in subtropical stratocumulus decks. *Atmospheric Chemistry and Physics*, *20*(6), 3609–3621. doi: 10.5194/acp-20-3609-2020

Stephens, G. L., Li, J., Wild, M., Clayson, C. A., Loeb, N., Kato, S., ... Andrews, T. (2012). An update on earth's energy balance in light of the latest global observations. *Nature Geoscience*, *5*, 691–696. doi: 10.1038/ngeo1580

Stevens, B., & Feingold, G. (2009). Untangling aerosol effects on clouds and precipitation in a buffered system. *Nature*, *461*, 607–613. doi: 10.1038/nature08281

Su, W., Corbett, J., Eitzen, Z., & Liang, L. (2015). Next-generation angular distribution models for top-of-atmosphere radiative flux calculation from CERES instruments: methodology. *Atmospheric Measurement Techniques*, *8*(2), 611–632. doi: 10.5194/amt-8-611-2015

Toll, V., Christensen, M., Quaas, J., & Bellouin, N. (2019). Weak average liquid-cloud-water response to anthropogenic aerosols. *Nature*, *572*, 51–55. doi: 10.1038/s41586-019-1423-9

Trofimov, H., Bellouin, N., & Toll, V. (2020). Large-scale industrial cloud perturbations confirm bidirectional cloud water responses to anthropogenic aerosols. *Journal of Geophysical Research: Atmospheres*, *125*(14), e2020JD032575. doi: https://doi.org/10.1029/2020JD032575

Twomey, S. (1974). Pollution and the planetary albedo. *Atmospheric Environment*, *8*(12), 1251–1256. doi: 10.1016/0004-6981(74)90004-3

Twomey, S. (1977). The influence of pollution on the shortwave albedo of clouds. *J. Atmos. Sci.*, *34*(7), 1149–1152. doi: 10.1175/1520-0469(1977)034⟨1149:TIOPOT⟩2.0.CO;2

Wang, S., Wang, Q., & Feingold, G. (2003). Turbulence, condensation, and liquid water transport in numerically simulated nonprecipitating stratocumulus clouds. *Journal of the Atmospheric Sciences*, *60*(2), 262–278. doi: 10.1175/1520-0469(2003)060⟨0262:TCALWT⟩2.0.CO;2

Wielicki, B. A., Barkstrom, B. R., Harrison, E. F., Lee, R. B., Smith, G. L., & Cooper, J. E. (1996). Clouds and the Earth's Radiant Energy System (CERES): An Earth Observing System Experiment. *Bulletin of the American Meteorological Society*, *77*(5), 853–868. doi: 10.1175/1520-0477(1996)077⟨0853:CATERE⟩2.0.CO;2

Wood, R. (2007). Cancellation of aerosol indirect effects in marine stratocumulus through cloud thinning. *Journal of the Atmospheric Sciences*, *64*(7), 2657–2669. doi: 10.1175/JAS3942.1

Wood, R. (2012). Stratocumulus clouds. *Monthly Weather Review*, *140*(8), 2373–2423. doi: 10.1175/MWR-D-11-00121.1

Wyant, M. C., Bretherton, C. S., Rand, H. A., & Stevens, D. E. (1997). Numerical simulations and a conceptual model of the stratocumulus to trade cumulus transition. *J. Atmos. Sci.*, *54*(1), 168–192. doi: 10.1175/1520-0469(1997)054⟨0168:NSAACM⟩2.0.CO;2

Xue, H., & Feingold, G. (2006). Large-eddy simulations of trade wind cumuli: Investigation of aerosol indirect effects. *Journal of the Atmospheric Sciences*, *63*(6), 1605–1622. doi: 10.1175/JAS3706.1

Zhang, J., Zhou, X., Goren, T., & Feingold, G. (2022). Albedo susceptibility of northeastern pacific stratocumulus: the role of covarying meteorological conditions. *Atmospheric Chemistry and Physics*, *22*(2), 861–880. doi: 10.5194/acp-22-861-2022

Zhang, J., & Zuidema, P. (2021). Sunlight-absorbing aerosol amplifies the seasonal cycle in low-cloud fraction over the southeast atlantic. *Atmospheric Chemistry and Physics*, *21*(14), 11179–11199. doi: 10.5194/acp-21-11179-2021